



## TECHNICAL REPORT

## Groundwater Quality

## Phosphorus adsorption on iron-coated sand under reducing conditions

Victoria Barcala<sup>1,2</sup>  | Stefan Jansen<sup>3</sup>  | Jan Gerritse<sup>3</sup> | Stefan Mangold<sup>4</sup> |  
 Andreas Voegelin<sup>5</sup> | Thilo Behrends<sup>2</sup>

<sup>1</sup>Inland Water Systems, Deltares,  
 Daltonlaan 600, Utrecht, The Netherlands

<sup>2</sup>Dep. of Earth Sciences, Faculty of  
 Geosciences, Utrecht Univ., 8  
 Princetonlaan, Utrecht, The Netherlands

<sup>3</sup>Deltares, Unit Subsurface and  
 Groundwater Systems, Daltonlaan 600,  
 Utrecht, The Netherlands

<sup>4</sup>Karlsruhe Institute of Technology, Institute  
 for Photon Science and Synchrotron  
 Radiation, Eggenstein-Leopoldshafen,  
 Germany

<sup>5</sup>Eawag, Swiss Federal Institute of Aquatic  
 Science and Technology, Ueberlandstrasse  
 133, Duebendorf, Switzerland

## Correspondence

Victoria Barcala, Inland Water Systems,  
 Deltares, Daltonlaan 600, 3584 BK Utrecht,  
 The Netherlands.

Email: [victoria.barcapaoilillo@deltares.nl](mailto:victoria.barcapaoilillo@deltares.nl)

Assigned to Associate Editor Nora Casson.

## Funding information

P-TRAP Marie Skłodowska-Curie Actions,  
 Grant/Award Number: EU Grant No.  
 813438

## Abstract

Mitigation measures are needed to prevent large loads of phosphate originating in agriculture from reaching surface waters. Iron-coated sand (ICS) is a residual product from drinking water production. It has a high phosphate adsorption capacity and can be placed around tile drains, taking no extra space, which increases the farmers' acceptance. The main concern regarding the use of ICS filters below groundwater level is that limited oxygen supply and high organic matter concentrations may lead to the reduction and dissolution of iron (hydr)oxides present and the release of previously adsorbed phosphate. This study aimed to investigate phosphate adsorption on ICS at the onset of iron reduction. First, we investigated whether simultaneous metal reduction and phosphate adsorption were relevant at two field sites in the Netherlands that use ICS filters around tile drains. Second, the onset of microbially mediated reduction of ICS in drainage water was mimicked in complementary laboratory microcosm experiments by varying the intensity of reduction through controlling the oxygen availability and the concentration of degradable organic matter. After 3 yr, ICS filters in the field removed phosphorus under low redox conditions. Over 45 d, the microbial reduction of manganese and iron oxides did not lead to phosphate release, confirming field observations. Electron microscopy and X-ray absorption spectroscopy did not evince systematic structural or compositional changes; only under strongly reducing conditions did iron sulfides form in small percentages in the outer layer of the iron coating. Our results suggest that detrimental effects only become relevant after long periods of operation.

**Abbreviations:** DOC, dissolved organic carbon; IC, ion chromatography; ICS, iron-coated sand; LCF, linear combination fitting; SEM, scanning electron microscopy; SEM-EDX, scanning electron microscopy with energy dispersive X-ray spectroscopy; TDP, total dissolved phosphorus; XAS, X-ray absorption spectroscopy.

This is an open access article under the terms of the [Creative Commons Attribution-NonCommercial](https://creativecommons.org/licenses/by-nc/4.0/) License, which permits use, distribution and reproduction in any medium, provided the original work is properly cited and is not used for commercial purposes.

© 2022 The Authors. *Journal of Environmental Quality* published by Wiley Periodicals LLC on behalf of American Society of Agronomy, Crop Science Society of America, and Soil Science Society of America.

# 1 | INTRODUCTION

Phosphorus (P) is an essential nutrient for plant growth, required to increase the food available for the growing world population. However, P runoff and leaching from agriculture can trigger algae blooms, eutrophication, and water quality problems (Bol et al., 2018; Withers & Haygarth, 2007). Due to the legacy of P in the soil, reducing fertilizer application may be insufficient to reduce the P load to surface waters in the short- to mid-term (Barcala et al., 2020; Chardon & Schoumans, 2007; Mellander et al., 2016; Sharpley et al., 2013). To achieve a faster decrease in the P levels in surface waters, we need mitigation measures that reduce the diffuse P inputs from arable fields (Mendes, 2020; Penn et al., 2017; Schoumans et al., 2014). These mitigation measures should be cost-efficient and make no or little use of valuable arable land to be readily accepted by farmers. Iron-coated sand (ICS) is a phosphate ( $\text{PO}_4$ ) adsorbing material, which is readily available as a by-product of drinking water production (Chardon et al., 2012; Sharma et al., 2002; Van Beek et al., 2020) and can be placed around tile drains or in edge-of-field filters to remove  $\text{PO}_4$ , taking no extra space (Chardon et al., 2021; Groenenberg et al., 2013; Lambert et al., 2020; Vandermoere et al., 2018). The iron (Fe) in the ICS coating is formed around sand particles at the top of rapid sand filters when they remove the suspended Fe (hydr)oxides that are formed upon the aeration of anoxic Fe(II)-containing groundwater or after the addition of Fe salts to remove organic matter. The ICS combines favorable adsorption properties with a high hydraulic conductivity. These properties together with its abundant availability at a low cost make ICS a suitable material for large-scale  $\text{PO}_4$  removing filters (Chardon et al., 2012; Vandermoere et al., 2018).

The major concern about the use of ICS filters below groundwater level is that the reductive dissolution or the reductive transformation of Fe (hydr)oxides over time may eventually lead to the release of previously retained  $\text{PO}_4$ . When drains are below the groundwater level, the oxygen supply is limited. The absence of oxygen and the presence of dissolved organic matter can enable anaerobic dissimilation, in which microorganisms use nitrate ( $\text{NO}_3$ ), manganese (Mn) and Fe (hydr)oxides, sulfate ( $\text{SO}_4$ ), and/or  $\text{CO}_2$  as terminal electron acceptors. The redox sensitivity of Fe has been identified as the primary reason for the mobilization of  $\text{PO}_4$  in natural environments under suboxic or anoxic conditions (Schroth et al., 2015; Thamdrup, 2000; Young & Ross, 2001). In addition, previously adsorbed or co-precipitated  $\text{PO}_4$  may be released when amorphous Fe(III)-(hydr)oxides continue to polymerize or transform into more crystalline forms such as goethite, possibly catalyzed by dissolved Fe(II) (Kraal et al., 2019; Pedersen et al., 2005; Senn et al., 2017). On the other hand, at the onset of Fe reduction,  $\text{PO}_4$  release may be com-

## Core Ideas

- After 3 years in the field ICS filters removed P under Mn and Fe reducing conditions.
- We studied the effect of reducing conditions on P adsorption on ICS with microcosm experiments.
- For 45 days under different reducing conditions, P was not released after Mn and Fe partial reduction.
- Most of the crystal structure of the ICS remained unchanged despite Mn and Fe reduction.

pensated by re-adsorption onto Fe (hydr)oxides that have not been reduced yet or by uptake into transformation products such as vivianite or mixed-valence Fe(II/III) oxides (Baken et al., 2016; Borch & Fendorf, 2008; Heiberg et al., 2012; Szilas et al., 1998; Van der Grift et al., 2016).

Groenenberg et al. (2013) and Chardon et al. (2021) performed a long-term experiment on the  $\text{PO}_4$ -removing efficiency of ICS-enveloped tile drains in a flower-bulb field in the Netherlands. The flower-bulb area is characterized by intensive agriculture, calcareous sandy soils with low P binding capacity, and P- and Fe(II)-rich seepage (Griffioen, 1994). In Chardon et al. (2021), after 26 mo, higher Fe levels were found in the effluent of the ICS-enveloped drains than in reference drains, which indicated that microbial metal reduction was occurring. During the first 26 mo of operation, Mn concentrations were high in the effluent of ICS enveloped drains. Manganese (hydr)oxides are energetically more favorable as electron acceptors than Fe (III)-(hydr)oxides. Manganese (hydr)oxide reduction may occur by microbial respiration of Mn(IV) or by abiotic reduction of Mn(IV) by Fe(II) (Postma & Appelo, 2000). The Fe(II) may be produced by microbial respiration in the filter or be already present in the groundwater. Manganese made up about 0.4% of the dry weight in most ICS (Groenenberg et al., 2013; Sharma et al., 2002). Despite ongoing Fe reduction and dissolution of Fe(III)-(hydr)oxides, the ICS-enveloped tile drains still removed on average 93% of the dissolved P after 54 mo of operation. These results suggested that (a) the rates of Fe reduction in the ICS filter depended on the rates of organic matter oxidation and the availability of electron acceptors and (b) the onset of Fe reduction did not necessarily cause the release of  $\text{PO}_4$  or loss of  $\text{PO}_4$  removal efficiency.

The objective of this study was to expand earlier field observations with new field sites and well-controlled laboratory tests to better constrain the effect of emerging reducing conditions on the performance of ICS in filter systems used to reduce the  $\text{PO}_4$  export from agricultural areas. For this, we (a) investigated two sites in the flower-bulb growing area of the Netherlands where ICS-enveloped drains have been

installed since 2018 for  $\text{PO}_4$  removal to assess whether simultaneous metal reduction and  $\text{PO}_4$  adsorption occurred and (b) performed microcosm experiments to mimic the onset of microbially-mediated reduction of ICS in drainage water by varying the intensity of reduction though controlling the oxygen availability and the concentration of degradable organic matter. The findings of this research provide a better understanding of the behavior of ICS under reducing conditions. This is relevant for the implementation of ICS filters, as previous research mainly focused on the adsorption capacity of the ICS and not on its stability under reducing conditions.

## 2 | MATERIALS AND METHODS

### 2.1 | Field sites

Two sites in the flower-bulb growing region of the Netherlands were investigated. The region has poor sandy soils, and the farmers add a mix of compost and straw as fertilizer, which are sources of  $\text{PO}_4$  and organic matter; these conditions combined result in a high risk for P leaching. At the two sites, ICS-enveloped drains were constructed in 2018 to reduce the  $\text{PO}_4$  loads to surface waters. Iron-coated sand was placed around the drains following the previous experiment by Groenenberg et al. (2013) and a pilot study by Buijert et al. (2015) where the ICS around drains performed better than two end-of-pipe filters. After the construction of the systems used in this study, successful end-of-pipe filters were reported by Lambert et al. (2020) and Vandermoere et al. (2018). If there is space and enough hydraulic head available in the ditch, end-of-pipe filters offer the advantage of being easier to replace with new material and the redox conditions may be less extreme. Field A is located in Noordwijkerhout ( $52^\circ 15' 52''$  N;  $4^\circ 30' 25''$  W) and Field B is in Vogelenzang ( $52^\circ 19' 44''$  N;  $4^\circ 34' 52''$  W). The total area drained in Field A is 7 ha and in Field B 12 ha. In both fields, about 0.015  $\text{m}^3$  of ICS was added per linear meter of drain ( $\sim 26.5$  kg ICS/m) without mechanical packing. The drains were constructed every 10 m, placed 90 cm below surface, and the groundwater level is kept at around 60 cm. The drains are connected to a main drain that discharges into a pumping station with a float-activated pump that maintains a constant the groundwater level by discharging into a ditch. The average annual rainfall between 2019 and 2021 was about 860 mm (Royal Netherlands Meteorological Institute, 2022). The drains remove excess infiltrating rainwater and upwelling groundwater. The estimated groundwater seepage in Field A is between 0.10 and 1.0 mm/d, and in field B it is between 0.10 and 0.25 mm/d (Janssen et al., 2020). In the summer, evapotranspiration is higher than precipitation and there is no need to continuously pump water out of the field; instead, the drains are used for irrigation, the level in the ditch is elevated, and

oxic water infiltrates from the ditch into the field. Unlike the field studied by Groenenberg et al. (2013) and Chardon et al. (2021) where water flowed freely to the ditch, Fields A and B use pumps to keep the groundwater levels constant. A video of the construction of the ICS enveloped drains is included in the Supplemental Material.

To investigate the relationship between redox conditions and P retention at the field scale, Fields A and B were sampled four times, from June 2019 to October 2020. Each time, a piezometer standpipe with a perforated bottom covered with a cloth filter was used to take one groundwater sample in the middle of the field 60 to 100 cm below ground level. A second sample was taken from the outflow of the main drain. Samples were not taken during summer since water was not flowing out of the drains. The samples were filtered ( $0.45 \mu\text{m}$ ) and total dissolved phosphorus (TDP), Fe, Mn,  $\text{NO}_3$ , and ammonium ( $\text{NH}_4$ ) were measured. The oxidation-reduction potential (ORP) and pH were measured on-site with a sensor (GMH3511, Geisinger) in a flow-through system. Dissolved organic carbon (DOC) was measured with the combustion catalytic oxidation method (TOC-V, Shimadzu). Shallow groundwater can be redox stratified and not be representative of the composition of drainage water entering the drains. Therefore, in August 2021, a gas vapor probe (GVP, Kit w/ DeWALT D25600K Hammer Drill, AMS) was used to make a depth-concentration profile in the groundwater below the drains. A gas vapor probe has a metal tip with a filter and extensions that are drilled in the soil to take water samples at precise depths. Samples were taken about every 30 cm from 100-to-380-cm depth and filtered ( $0.45 \mu\text{m}$ ) into a pre-acidified tube on-site to measure TDP, Fe, and Mn.

### 2.2 | Laboratory experiment

#### 2.2.1 | Starting materials

The groundwater used for microcosms experiments was collected from a third field, located in Noordwijkerhout ( $52^\circ 15' 38''$  N;  $4^\circ 28' 46''$  W). This field is 1000 m apart from Field A and has similar soil and flower production characteristics but does not have ICS filters around the drains. The groundwater composition, before starting the experiment and after being stored for 1 wk in the dark at  $4^\circ\text{C}$  under oxic conditions, was 19.5 mg/L of DOC, 0 mg/L acetate, 8.3 mg-P/L TDP, 10.6 mg-N/L  $\text{NH}_4$ , 0.9 mg-N/L  $\text{NO}_3$ , 3.4 mg-S/L  $\text{SO}_4$ , 65.2 mg/L Ca, 0.09 mg/L Mn, and 0.03 mg/L Fe. We used the same analytical methods as for the other groundwater samples.

The ICS used for the microcosms and the field filters is a by-product of groundwater iron removal by aeration during drinking water production. Both ICS were obtained from AquaMinerals BV (<https://aquaminerals.com/en/>), a company

that develops sustainable chains for by-products of the water treatment process. Because the material from the batch used in the construction of the ICS enveloped drains was no longer available, the ICS used was from a different batch. The ICS used for the microcosms was air-dried and stored in the dark with no additional washing or pretreatment and characterized by total extraction, scanning electron microscopy with energy dispersive X-ray spectroscopy (SEM–EDX), and X-ray absorption spectroscopy (XAS). It contained on average 127.0 mg/g Fe, 9.4 mg/g Mn, 0.5 mg/g S, 9.6 mg/g Ca, and 0.9 mg/g P ( $\pm 0.1$  mg/g SD), implying that the molar P/Fe ratio of the fresh ICS was  $\sim 0.013$ . The grain size distribution of the ICS batch received from Aquaminerals was  $D_{10}$ , 0.46 mm and  $D_{60}$ , 2.11 mm (Supplemental Figure S8). The maximum porosity was 0.50 and the minimum was 0.39. The saturated hydraulic conductivity at the lowest porosity was  $5.5 \times 10^{-3}$  cm/s, and the bulk density was 1770 kg/m<sup>3</sup>. As for the maximum P adsorption capacity, Chardon et al. (2012) calculated 18.7 mg/g Fe for iron by-products obtained from drinking water treatment plants in the Netherlands, equivalent to a 0.10 P/Fe molar ratio.

## 2.2.2 | Microcosm experiments

In the microcosm experiments, we aimed to capture the onset of weakly, moderately, and strongly reducing conditions and to have similar P concentrations and P loadings as in the field setting. The initial TDP concentration of 8.3 mg P/L is close to the highest values we have measured in the field. We decided not to pre-load the ICS with P. Chardon et al. (2021) measured with total extractions that the P/Fe molar ratio of the ICS in the field had only marginally increased from 0.030 to 0.033 after 59 mo of operation. That is, the dominant P pool of ICS used in the field was still the P inherited from production and the additionally adsorbed P represented only a minor fraction. The P originally present in the ICS is likely on the inside of the coating and the freshly adsorbed P on the outside of the coating. Therefore, we assume that freshly adsorbed P is most prone to be released under reducing conditions. Consequently, we used groundwater with relatively high TDP concentration to create freshly adsorbed P in our experiments.

The intensity of reduction in the microcosms was modulated by introducing acetate as a carbon and electron source and by varying the availability of dioxygen (O<sub>2</sub>). This allowed us to investigate the fate of PO<sub>4</sub> partitioning in the ICS at different rates of microbial respiration in the presence of alternative electron acceptors to Fe (hydr)oxides such as O<sub>2</sub>, NO<sub>3</sub>, Mn (hydr)oxides, and SO<sub>4</sub>. Four different treatments were investigated:

1. Strongly reducing conditions were introduced by closing the bottles, replacing the headspace with 95% N<sub>2</sub> and 5% CO<sub>2</sub>, and stimulating microbial respiration by adding acetate as an electron donor.
2. Moderately reducing conditions were introduced by allowing the resupply of O<sub>2</sub> via diffusion through the headspace that was kept unaltered with atmospheric composition and adding acetate as an electron donor.
3. Weakly reducing conditions were introduced by replacing the headspace with 95% N<sub>2</sub> and 5% CO<sub>2</sub> and omitting the addition of acetate. The same amount of deionized anoxic water as from the acetate stock solution was added to maintain an equal dilution as in the other treatments. The DOC present in the groundwater was the only available electron donor.
4. Abiotic controls were autoclaved (20 min, 121 °C) on Day 1 to prevent microbiologically induced electron transfer. The headspace was replaced with 95% N<sub>2</sub> and 5% CO<sub>2</sub>, and acetate was added.

Each treatment was done in triplicate in 250-ml glass bottles with 30 g of ICS and 80 ml of groundwater. The groundwater was flushed with CO<sub>2</sub> containing anoxic gas (95% N<sub>2</sub> and 5% CO<sub>2</sub>) to use the carbonate system as a pH buffer. This was done for all treatments, including the one with air in the headspace, to achieve a comparable starting pH. Immediately before sealing the bottles, the pH was measured with a semi-microprobe (877 Metrohm Titrino) and was  $6.8 \pm 0.3$ . After the bottles were sealed, the pH was checked by placing one drop on pH paper. Only small pH differences were observed after acetate addition (Supplemental Table S3). The bottles were sealed with butyl rubber stoppers and incubated horizontally in the dark for 45 d at  $20 \pm 1$  °C with no mechanical shaking besides the movement introduced by sampling. The temperature chosen was higher than the measured field temperatures and conservative with respect to the extent of microbial reduction in the field.

To represent the onset of the different reducing conditions, enough acetate was added to stoichiometrically reduce one-third of the Fe in the ICS if the entire acetate was respired using Fe(III) as an electron acceptor. The acetate was introduced by injecting 3 ml of a 0.95 mol/L sodium acetate solution, giving a final acetate concentration of 2.27 g/L (2.88 mmol) in the corresponding bottles. On Day 10 when the acetate was added, the initially present TDP was largely adsorbed by the ICS (corresponding to a molar  $P_{\text{ads}}/\text{Fe}$  of  $\sim 0.00035$ ) and residual TDP was below  $0.006 \pm 0.003$  mg P/L. The P originally present in the ICS was still the most important fraction ( $P_0/\text{Fe}$  of  $\sim 0.013$ ).

The bottles were sampled three times per week. Aqueous samples were taken with a needle (0.5 × 25 mm) and a syringe. Before sampling, the syringe was prefilled with the same gas as in the headspace of the bottles and a volume of 2.5 ml of gas was injected to maintain the pressure in the bottles and avoid O<sub>2</sub> intrusion. The samples were directly filtered (0.45 μm),



and 1 ml was placed on a 2-ml tube (Eppendorf) containing 100  $\mu$ l of nitric acid (14 M) for photometric measurements. On three occasions, an extra 1 ml sample without acid was taken for IC measurements. On Day 31, additional P was added to a concentration of  $1.00 \pm 0.05$  mg P/L to all the bottles to assess the adsorption after the ICS has been subjected to microbial reduction, and microbial activity is expected to have declined.

## 2.2.3 | Analytical techniques

Dissolved Fe(II) and total dissolved Fe were determined photometrically with an acetate buffered phenanthroline solution at 510 nm (Saywell & Cunningham, 1971). For total dissolved Fe, the samples were pre-reduced with hydroxylammonium chloride. Total dissolved Mn was determined photometrically with hydroxylamine, formaldehyde, and ammonium hydroxide, at 450 nm (Brewer & Spencer, 1969). Total dissolved P was measured photometrically at 880 nm after 30 min of incubation with ammonium heptamolybdate solution acidified with sulfuric acid and freshly added ascorbic acid (Murphy & Riley, 1962). Acetate,  $\text{NH}_4$ , Ca,  $\text{NO}_3$ , and  $\text{SO}_4$  were measured in non-acidified filtered samples with ion chromatography (ICS-6000, Thermo Scientific). The ICS-6000 has two columns to perform anion and cation analysis at 30 and 60  $^{\circ}\text{C}$ , respectively. The equipment has an autosampler and eluent generator that uses a standard potassium hydroxide solution for cations and a meta-sulfuric acid solution for anions together with freshly produced Milli-Q water (Advantage, A10, Merk).

For the total extraction, the ICS was ground using an agate mortar, 0.125 g of sample was weighed into a vessel, and 2.5 ml of a mixture of  $\text{HClO}_4$  (72%) and  $\text{HNO}_3$  (65%) with a 3:2 volume ratio and 2.5 ml HF (48%) were added. After being left overnight at 90  $^{\circ}\text{C}$ , the vessel was heated at 140  $^{\circ}\text{C}$  for 4 h to evaporate the liquids. Then, 25 ml of  $\text{HNO}_3$  was added and the samples were left once again overnight at 90  $^{\circ}\text{C}$ . After filtration (0.45  $\mu\text{m}$ ), the solution was analyzed with inductively coupled plasma–optical emission spectrometry (Avio 500, Perkin-Elmer). The extraction was done in duplicate.

We used XAS to characterize the Fe in the ICS before and after the different treatments. To obtain samples with an edge-step of around unity in transmission spectra, 10 mg of ICS was air-dried, ground, mixed with 40 g of cellulose, and pressed into 7-mm-diam. pellets. To prevent oxidation artifacts during sample preparation, all manipulations were performed in a glove box. For storage and transport, the pellets were placed in sealed aluminum bags under an inert  $\text{N}_2$  atmosphere. The fresh ICS was measured at the SuperXAS beamline at the Swiss Light Source (SLS, Paul Scherer Institute, Villigen, Switzerland) at room temperature. The treated samples were measured at the XAS beamline at the KIT Light Source at the Karlsruhe Institute of Technology (KIT; Germany) under

vacuum. Based on a preliminary inspection of the sample spectra, the following reference spectra were included: (a) silicate-containing ferrihydrite (Fh-Si) formed by the oxidation of Fe(II) in bicarbonate-buffered silicate-containing synthetic groundwater, (b) 2-line ferrihydrite (2L-Fh) synthesized by the forced hydrolysis of a concentrated ferric iron solution (Schwertmann & Cornell, 2000) (both spectra from Senn et al., 2017), and (c) mackinawite ( $\text{FeS}$ ; spectrum kindly provided by Mingkai Ma, Utrecht University). For data extraction and evaluation by linear combination fitting (LCF), the software code Athena was used (Ravel & Newville, 2005).

We used SEM–EDX to observe the ICS grains before and after the different microcosm treatments. The ICS grains were embedded in resin and polished to investigate cross-sections of the Fe coating. Samples were mounted directly on 1.25-cm aluminum stubs using double-sided carbon adhesive stickers. No platinum coating layer was used as it can interfere with P detection. Secondary electron and backscattered electron images were acquired on a Zeiss EVO 15 SEM, using the SmartSEM user interface (v. 6.06). Qualitative (or semi-quantitative) chemical compositions were obtained using a Bruker XFlash EDS system (Esprit v. 2.1). The electric high tension (EHT), scale, and working distance are indicated on the images.

## 3 | RESULTS

### 3.1 | Field results

The composition of the shallow groundwater varied considerably between the four sampling campaigns (Table 1). Total dissolved P was consistently lower in the drain outflow than in the shallow groundwater at all sampling dates. In contrast, Fe and Mn concentrations were higher in the drain outlet compared with the shallow groundwater at all sampling dates, except for 14 Oct. 2020. The influence of the deeper groundwater on the drained water can be seen, for example, in the  $\text{NH}_4$  concentrations (Table 1; Figure 1; Supplemental Table S4). In the deep groundwater, Fe and Mn concentrations showed the general tendency to increase with depth and were higher than in the shallow groundwater at both field sites (Figure 1; Supplemental Table S4). The TDP concentrations were higher in the deep groundwater in Field A than in B and the TDP removal calculated taking the shallow groundwater as reference was lower in Field A than in B.

### 3.2 | Dynamics of solution composition in microcosm experiments

Changes in dissolved concentrations in the four different microcosms are shown in Figure 2 and Supplemental

**TABLE 1** Concentrations in the shallow groundwater above iron-coated sand-enveloped drains, 60–100 cm below the surface, and in the drain outflow in Fields A and B of dissolved (0.45 µm) Fe, Mn, total dissolved P (TDP), dissolved organic C (DOC), electrical conductivity (EC), oxidation reduction potential (ORP), NO<sub>3</sub><sup>-</sup>, and NH<sub>4</sub><sup>+</sup>

Date	11 June 2019 Field A shallow groundwater	9 Dec. 2019	7 Feb. 2020	14 Oct. 2020	11 June 2019 Field A drain outflow	9 Dec. 2019	7 Feb. 2020	14 Oct. 2020
Fe (mg/L)	0.03	0.02	0.04	0.95	0.03	0.11	1.1	0.05
Mn (mg/L)	0.8	1.4	1.1	1.6	3.9	2.4	2.6	5.0
TDP (mg P/L)	0.68	7.1	3.2	2.0	0.34	3.6	1.2	0.4
TDP retention (%) <sup>a</sup>					50	50	63	80
NO <sub>3</sub> (mg N/L)	<0.02	<0.02	<0.02	<0.02	<0.02	<0.02	<0.02	<0.02
NH <sub>4</sub> (mg N/L)	0.9	4.0	1.3	2.1	3.2	4.9	4.9	3.9
DOC (mg/L)	15.7	19.1	11.5	24.4	15.4	20.6	15.3	20.1
EC (µS/cm)	1700	1300	1100	1500	1200	1100	1000	1200
Temp. (°C)			5	12.7			6	13
pH			7.1	6.9			7	7.2
ORP (mV)			−160	−194			−96	95
	<b>Field B shallow groundwater</b>				<b>Field B drain outflow</b>			
Fe (mg/L)	0.05	0.04	0.44	0.06	0.05	0.71	1.3	0.24
Mn (mg/L)	0.1	0.4	0.2	0.6	1.2	1.4	1.1	1.4
TDP (mg P/L)	2.2	4.0	4.3	3.7	0.34	0.41	0.38	0.32
TDP retention (%) <sup>a</sup>					85	90	91	91
NO <sub>3</sub> (mg N/L)	4.5	0.09	<0.02	2.6	<0.02	<0.02	<0.02	<0.02
NH <sub>4</sub> (mg N/L)	<0.04	0.08	0.23	0.08	1.8	1.8	1.6	1.6
DOC (mg/L)	23.2	31.6	26.2	28.9	15.0	20.1	15.7	17.2
EC (µS/cm)	830	850	710	950	950	1000	910	940
Temp (°C)			5	13.5			6	13.4
pH			7	6.8			7	7.2
ORP (mV)			70	176			−105	−114

$$^a \text{TDP retention (\%)} = \frac{\text{TDP}_{\text{shallow groundwater}} - \text{TDP}_{\text{drain outflow}}}{\text{TDP}_{\text{shallow groundwater}}} \times 100.$$

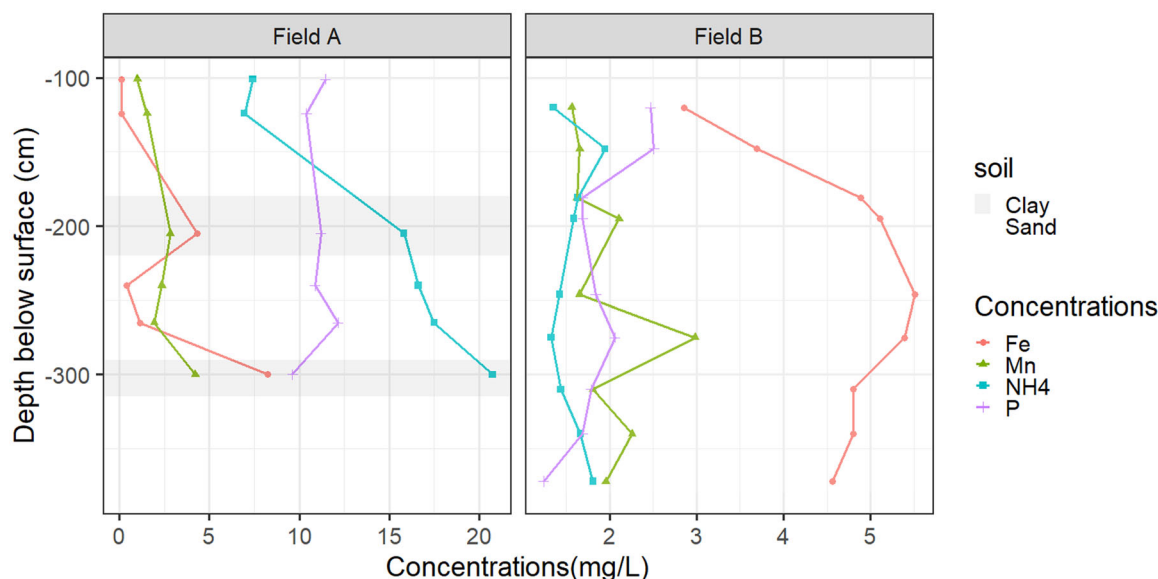


**FIGURE 1** Concentration profiles of dissolved (<0.45  $\mu\text{m}$ ) Fe, Mn,  $\text{NH}_4$ , and total dissolved P in the groundwater below the drains at Fields A and B. The groundwater level is at about  $-60$  cm depth; the drains are installed at around  $-90$  cm depth. Notice the different scales on the x axis. The clay and sand were classified on site while making the profiles based on the plasticity of the soil

Table S2. The addition of acetate induced microbially mediated metal reduction. Manganese concentrations peaked 2–4 d after acetate addition, increasing from  $0.09$  mg/L to  $24.8 \pm 2.0$  mg/L and  $10.3 \pm 1.7$  mg/L under strongly (no  $\text{O}_2$ ) and moderately (with  $\text{O}_2$  diffusion) reducing conditions, respectively. Only under strongly reducing conditions, Fe concentrations peaked 6 d after acetate addition around  $5.50 \pm 0.59$  mg/L and the color of the ICS changed from orange/brown to black (Supplemental Figure S2). The presence of DOC alone was not enough to induce an increase in Fe concentrations. Under weakly reducing conditions (only DOC was available as electron donor), the Mn concentration increased slightly to  $2.9 \pm 0.16$  mg/L and the decrease was not as pronounced as in the treatments with acetate addition. In the abiotic control, Mn concentrations increased abruptly on Day 2 (after the bottles were autoclaved) to values around  $9.7 \pm 0.6$  mg/L and stayed constant afterward throughout the experiment. The increase in Mn concentration was possibly caused by abiotic, thermally induced reduction of Mn oxides during autoclavation and possibly followed by disproportionation of Mn(III).

In all treatments, after  $\text{PO}_4$  adsorption onto the ICS, the  $\text{SO}_4$  concentration increased from  $3.4$  to  $9.8 \pm 2.0$  mg S/L. This was possibly caused by ligand exchange between  $\text{PO}_4$  and  $\text{SO}_4$  ions on adsorption sites. Under strongly reducing conditions, the  $\text{SO}_4$  concentrations eventually decreased to  $2.6 \pm 0.6$  mg S/L after 45 d, indicating microbial  $\text{SO}_4$  reduction. No P release was measured in any of the treatments. The P concentrations at the end of the experiment and after  $1.00 \pm 0.05$  mg P/L was added on Day 31 were  $0.09 \pm 0.03$  mg-P/L in strongly reducing conditions,

$0.005 \pm 0.02$  mg P/L in moderately reducing conditions, and  $0.003 \pm 0.001$  mg P/L in the weakly reducing conditions and in the autoclaved control.

Calcium,  $\text{NH}_4$ , and  $\text{NO}_3$  concentrations decreased at the end of the experiments in the microcosms under strongly and moderately reducing conditions. Calcium decreased from  $65.2$  mg/L to  $8.50 \pm 0.78$  mg/L and  $8.00 \pm 0.28$  mg/L, respectively. In both treatments,  $\text{NH}_4$  and  $\text{NO}_3$  were consumed. Under strongly reducing conditions both dropped to below detection ( $<0.02$  mg N/L), and under moderately reducing conditions  $\text{NH}_4$  decreased to  $1.8 \pm 0.1$  mg N/L and  $\text{NO}_3$  to  $0.02 \pm 0.01$  mg N/L. In both treatments, all acetate was consumed. Under weakly reducing conditions, the final  $\text{NH}_4$  was approximately half of the initial concentration,  $5.07 \pm 0.08$  mg N/L, and  $\text{NO}_3$  was  $0.02 \pm 0.01$  mg N/L. In the abiotic control, the acetate was not consumed, and  $\text{NH}_4$  and  $\text{NO}_3$  did not change. Water chemistry data are available in Supplemental Table S2.

### 3.3 | Characterization of solids from the microcosm experiment

Iron K-edge XAS was used to assess the speciation of Fe in the fresh and incubated ICS (see Supplemental Material; Supplemental Figure S1 and Supplemental Table S1). The Fe in the fresh ICS coatings was mainly contained in silicate-containing ferrihydrite, consistent with its accumulation by oxidation of Fe(II) in silicate-containing aerated groundwater (Senn et al., 2015), and in line with earlier XAS characterization results for Fe-sludge and ICS from drinking water

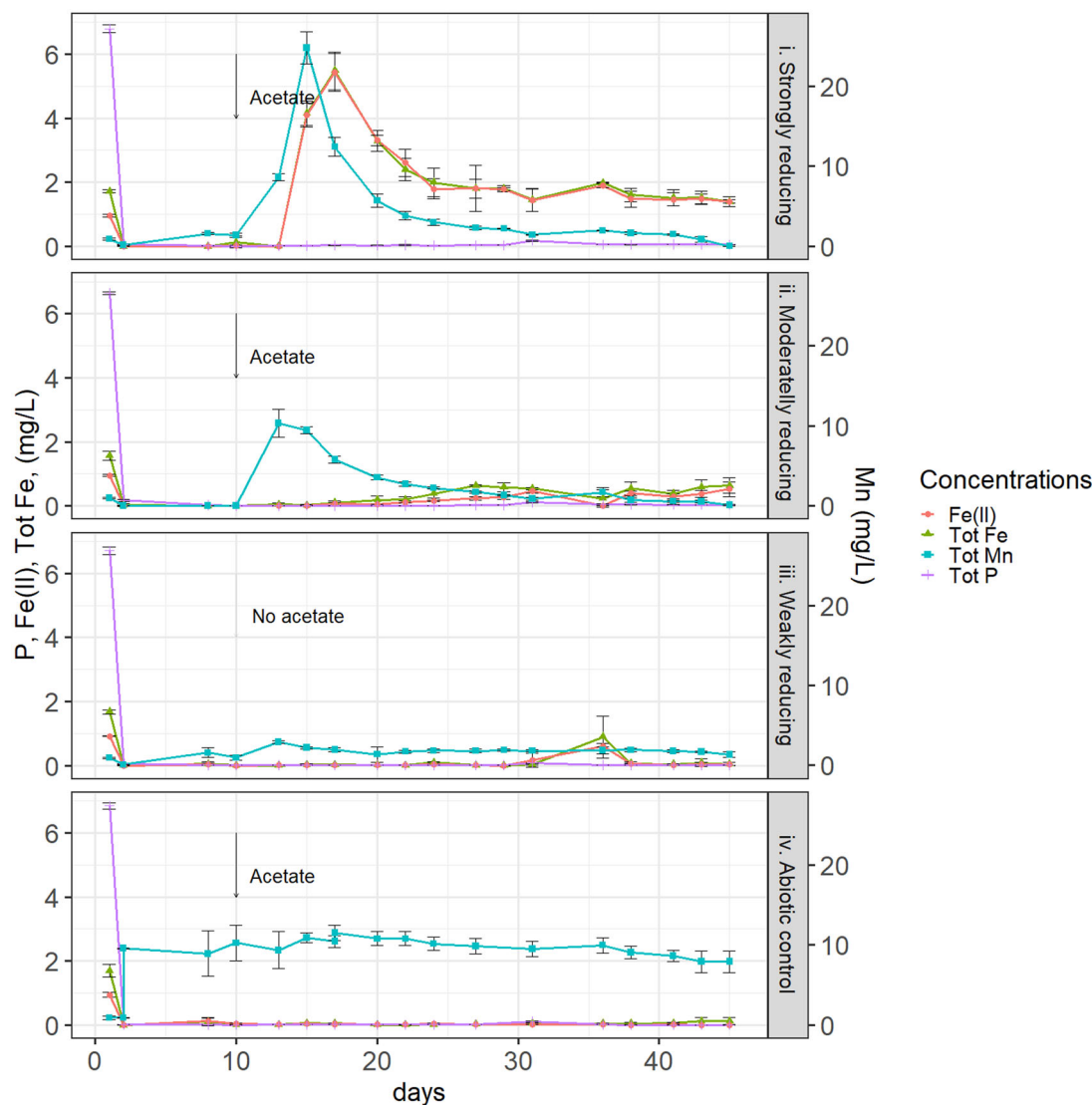


**FIGURE 2** Dissolved ( $<0.45\ \mu\text{m}$ ) concentrations of Fe(II), total Fe and Mn, and TDP in the microcosm experiments with iron-coated sand in groundwater at varying reducing conditions. In the bottles with acetate, 2.27 g/L was added on Day 10. In the abiotic control, the bottles were autoclaved on Day 1. The points are the mean, and the error bars indicate the standard deviation of three replicates

treatment (Chardon et al., 2021; Koopmans et al., 2020). Three of the reacted sample spectra closely matched the spectrum of the unreacted material, but one spectrum showed a spectral difference that was attributed to a contribution of 7% (X-ray absorption near-edge structure; XANES) to 13% (extended X-ray absorption fine structure; EXAFS) FeS based on LCF analysis. Although the four incubated samples were misplaced during pellet preparation or sample mounting in the glove box, this LCF result was attributed to the strongly reducing treatment (acetate, anoxic), which in contrast to the others showed clear signs of sulfidation, including a decrease in  $\text{SO}_4$  concentration during incubation and a change in color to black (Figure S2). The similarity of the Fe K-edge XAS spectra of the other three incubated samples to the spectrum of the fresh material indicated that silicate-containing ferrihydrite had not detectably transformed during incubation under

less reducing conditions in the absence of sulfide formation. This observation was in line with earlier results, suggesting that ICS deployed in a field did not detectably transform over 14 to 59 mo (Chardon et al., 2021).

Figure 3 shows the SEM images of the ICS. The ICS grains are larger than 1 mm in diameter, have a sand core, and have a 100-to-500- $\mu\text{m}$  coating composed of iron (hydr)oxides with a 1:3 average Fe/O ratio in a layered structure and regions of higher porosity and Mn contents (Figure 3a and 3b; Supplemental Figure S4). The P/Fe ratio measured with EDX was 0.015, which closely matches the total extraction results of the original ICS (Supplemental Figure S5). After the strongly reducing treatment, the grain surface transformed into a curved amorphous pattern (Figure 3e). Although S could not be detected with EDX, other researchers detected the same pattern when



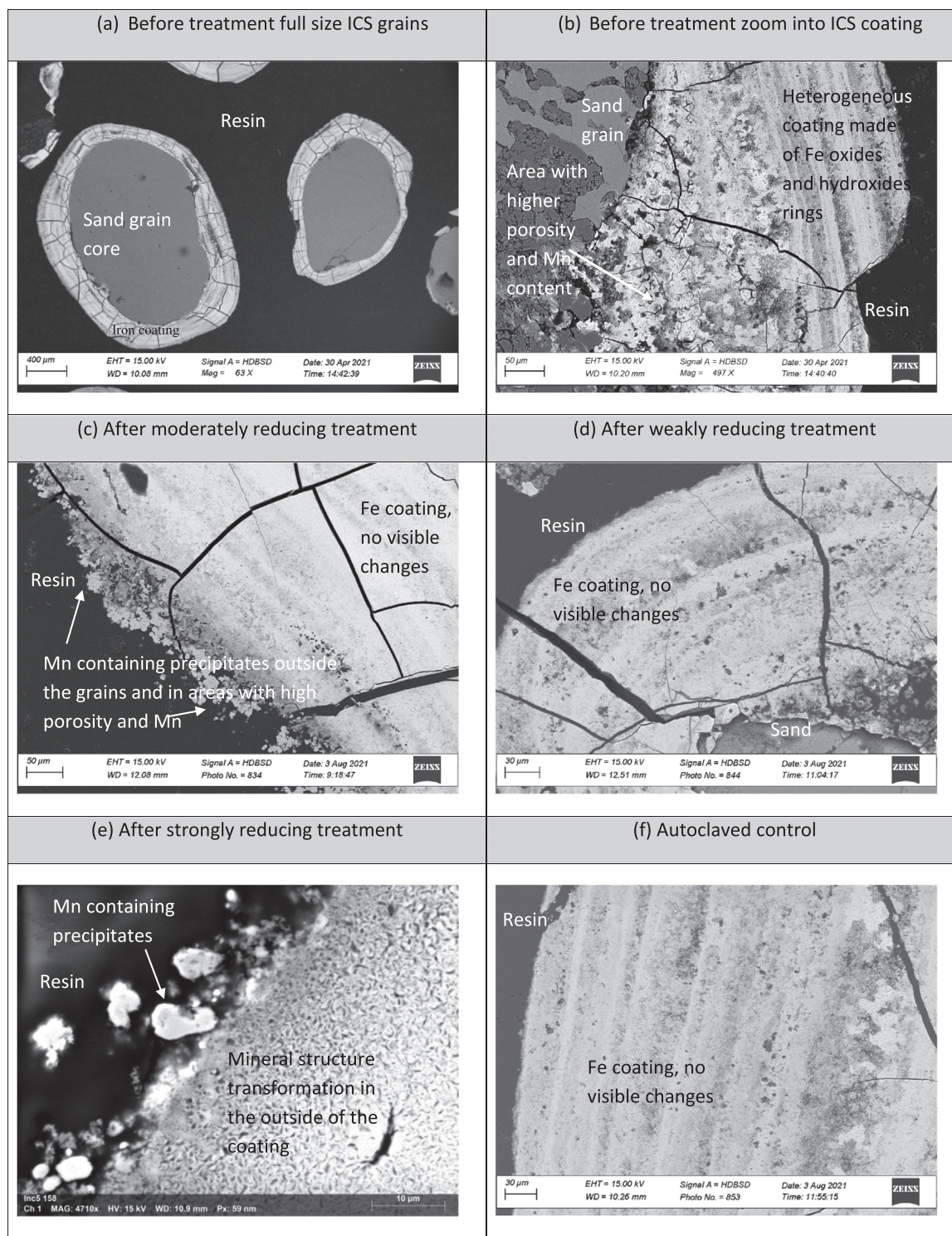


**FIGURE 3** Scanning electron microscopy (SEM) images of iron-coated sand (ICS) grains before treatment and after incubation in microcosms under a range of reducing conditions. Scale bars are indicated on each image. Most of the cracks that can be observed were most likely produced during the vacuum step of the SEM with energy dispersive X-ray spectroscopy

ferrihydrite was transformed into FeS (Akhtar et al., 2012; Csákbényi-Malasics et al., 2012; Zhang et al., 2021; Zou et al., 2018). In the samples from strongly and moderately reducing microcosms, precipitates with similar C/O/Ca/Mn ratios were seen in suspension close to the grains and inside

macropores (Figure 3c and 3d; Supplemental Figures S3, S6, and S7). The average C/O/Ca/Mn molar ratio obtained with EDX point measurements was 20 : 65 : 13 : 2. No major differences in the coating characteristics were detected in the abiotic control and after the weakly reducing treatment.

In the abiotic control, the autoclavation could potentially modify the structure of the iron (hydr)oxides; nevertheless, this sample looked similar to the original material under SEM–EDX and XAS, suggesting no major structural transformation occurred.

## 4 | DISCUSSION

### 4.1 | Fe and Mn reduction in ICS at the field sites and P retention

Removal of dissolved P from the drainage water by the ICS was indicated by consistently lower TDP concentrations in the drain outflow than in the groundwater at the same sampling event. Taking the concentrations in the shallow groundwater as a reference, the TDP removal efficiency varied between 50–80% and 85–91% in Fields A and B, respectively. One of the reasons for the lower removal in Field A may be the underestimation of the drainage water concentrations as the deeper groundwater had very high P concentrations. Although the field data suggests a significant TDP removal, it appears to be less effective than the TP removal observed by Chardon et al. (2021), who reported a 93% efficiency. Chardon et al. (2012) and Lambert et al. (2020) observed lower TDP removal efficiencies at higher flow velocities and at higher TDP inflow concentrations in ICS. The flow velocity was 60 cm/d in Chardon et al. (2021), while it was 180 cm/d at our sites. In field A, the lowest outflow TDP concentrations and highest removal efficiency coincided with Mn dissolution, suggesting TDP removal was not affected by metal reduction.

On most occasions, dissolved Fe concentrations were higher in the drain outflow than in the shallow groundwater but not higher than in deeper groundwater. For example, in February 2020, dissolved Fe concentrations were high in the drain outflow. This could be explained either by a larger contribution of deep groundwater in the drained water or by Fe reduction from the ICS. Therefore, without constraining the relative contribution of drainage water with different compositions to the drain outflow, it cannot be unambiguously concluded that Fe concentrations increased while flowing through the ICS. Although direct evidence for Fe reduction in the ICS layers at the two field sites is missing, NO<sub>3</sub> concentrations were consistently below the detection limit in the drain outflow, NH<sub>4</sub> concentrations were higher in the outflow than in the shallow groundwater, and there was a constant supply of electron donors in the form of DOC. Hence, in the absence of oxygen and nitrate, it is likely that the abundant Fe and Mn (hydr)oxides were used in the ICS layers as terminal electron acceptors by dissimilatory metal-reducing organisms. The reduction of Fe (hydr)oxides may lead to transformations in the solid phase and does not necessarily lead to an increase in dissolved Fe concentrations. The reduced Fe(II)

can be effectively adsorbed by Fe (hydr)oxides or form secondary minerals such as magnetite (Fe<sub>3</sub>O<sub>4</sub>), siderite (FeCO<sub>3</sub>), or iron sulfides.

Because it was difficult to quantify the importance of the metal reduction from the field data, we made an estimation of the metal reduction based on the stoichiometry of the reaction with DOC. When 12 g (1 mol) of C is oxidized going from C(0) to C(IV) oxidation state, four electrons are transferred to reduce 4 mol Fe(III) to Fe(II). As the drains are 10 m apart from each other, each linear meter of pipe drains 10 m<sup>2</sup>. We assumed that 70% of the precipitation surplus was transported through the drains, obtaining an annual flow of 3,215 L/m/yr [(860–450+36.5) mm × 10 m<sup>2</sup> × 70%], assuming the DOC concentration was 19.5 mg/L, the average TDP concentration in the drained water was 4.0 mg P/L, 73% TDP was retained, that there were originally 26.5 kg Fe per linear meter of drain, and all reduced Fe (II) was removed from the filter. It is possible to estimate the lifespan in years of the ICS filter before a 0.10 P/Fe molar ratio is reached with the following formula:

$$\frac{P}{Fe}_{(n_{\text{year}})} = \frac{P}{Fe}_0 + \frac{n_{\text{year}} \times 0.3 \text{ mol P/year/m}}{474 \text{ mol Fe/m} - \%_{\text{DOC}} \times n_{\text{year}} \times 20 \text{ mol Fe/year/m}} < 0.10$$

where P/Fe<sub>0</sub> is the original molar ratio in the ICS 0.013, *n* is the filter lifespan in years, %<sub>DOC</sub> is the percentage of DOC oxidized in the filter, 0.3 mol P/year/m is the P removal load per year, 474 mol Fe/m is the original amount of Fe, and 20 mol Fe/year/m is how much Fe we assume is lost per year.

We supposed two scenarios: one in which 100% of the DOC was respired using Fe (III)-(hydr)oxides as electron acceptors (which is not realistic, as part of the DOC is expected to be slowly or not degrading), and a more realistic case in which 10% of the DOC was respired. For these cases, 4 and 0.4% of the iron, respectively, would be reduced annually and a 0.10 P/Fe (III) molar ratio would be reached after 20 and 80 yr. These results are positive as drainage systems are traditionally designed for a lifespan between 20 and 40 yr (Skaggs et al., 1994). The remaining question is whether P release can also be expected at the onset of Fe and Mn reduction. For that reason, microcosm experiments were used to systematically investigate the dependency of P removal on microbially induced redox conditions in ICS.

### 4.2 | Phosphate release from ICS in microcosms at different reducing conditions

The metal reduction in the microcosms was microbially mediated as no changes occurred in the abiotic control after acetate addition. Manganese dissolved from ICS in the microcosms with moderately and strongly reducing conditions. Iron



dissolution only occurred in the microcosm with strongly reducing conditions when oxygen was not available and  $\text{SO}_4$  reduction in the water and solid phases occurred. Iron reduction affected the outer layer of the coating, which is likely where P was initially adsorbed, and the risk of P release is highest. However, even under strongly reducing conditions, neither the adsorbed P nor the P originally present in the ICS were mobilized into the overlying water in the microcosm experiments. These results are in agreement with the observation that P release upon reduction of P-loaded Fe (hydr)oxides can be effectively prevented if sufficient sorption sites remain available on unaltered Fe (hydr)oxides or secondary Fe minerals (Loeb et al., 2008; Smolders et al., 2017; Young & Ross, 2001). Our results do not allow us to identify a critical P/Fe ratio or, more specifically, a critical P/Fe (III) ratio at which P release cannot be effectively counteracted anymore. Nevertheless, considering the presence of silicate in the drainage water, a 0.1 ratio could be used (Hilbrandt et al., 2019). Our mass balance calculations point towards a potentially long lifespan before a 0.1 P/Fe(III) is reached.

The dynamics of dissolved Fe and Mn concentrations indicate the formation of Fe(II) and Mn(II) containing secondary products in the moderately and strongly reducing microcosms. The decrease in Mn concentration after an initial increase can be attributed to the formation of carbonate precipitates, possibly in the form of rhodochrosite ( $\text{MnCO}_3$ ) or as a solid solution with calcium carbonates. The newly formed carbonates were not part of the coating but formed precipitates in suspension or inside macropores. In contrast to Mn(II), Fe(II) was not enriched in carbonates but formed FeS, which remained associated with the Fe coating. Neither the carbonates nor FeS showed visible P enrichment in the SEM–EDX analyses, implying that the formation of secondary minerals did not significantly contribute to the retention of solid-bound P. Nevertheless, the formation of precipitates and microbial biomass could affect the performance of ICS filters by reducing the hydraulic conductivity and cause clogging. For instance, Vandermoere et al. (2018) observed a slight decrease in the hydraulic conductivity of ICS filters after 10 wk of use.

A minor FeS fraction formed in the strongly reducing microcosm. Microbial  $\text{SO}_4$  reduction can happen before or simultaneously with Fe(III) reduction. Sulfate-reducing bacteria such as *Desulfotomaculum* spp. use acetate as a carbon source and Fe(III) can be reduced by sulfide or by iron-reducing bacteria such as *Geobacter* spp. that also use acetate as a carbon source (Hansel et al., 2015; Islam et al., 2004; Kwon et al., 2016). The acetate added to each bottle was 2.85 mmol, which, upon oxidation to  $\text{CO}_2$ , should have been enough to reduce one-third of the initial metal (hydr)oxides present [22.8 mmol of Fe(III) to Fe(II) or 11.4 mmol of Mn(IV) to Mn(II)]. Only 0.04 and 1.54% of the initially added Fe and Mn, respectively, was recovered in reduced form in solution. This suggests that most electrons released by acetate

reduction were consumed by  $\text{SO}_4$  reduction or by the formation of solid-bound reduced metals. Based on XAS analyses, 7 to 13% (corresponding to 4.77 and 8.86 mmol) of the Fe transformed into FeS in these microcosms, which accounts for most of the acetate consumption [0.57 to 1.05 mmol for Fe(III) reduction and 0.91 to 1.68 mmol  $\text{SO}_4$  reduction]. Although these calculations close the electron balance, XAS may be overestimating the FeS fraction as it is not consistent with the sulfur mass balance based on the change in dissolved  $\text{SO}_4$ . Furthermore, nitrogen was consumed, possibly in processes involving oxidation of  $\text{NH}_4$  to  $\text{N}_2$ ,  $\text{NO}_2^-$ , or  $\text{NO}_3^-$  by iron-reducing bacteria (Feammox, Zhu et al., 2022), denitrification, and assimilation in biomass. Iron was in excess; if all the  $\text{NH}_4$  was transformed to  $\text{NO}_3^-$  and then denitrified, this could have reduced 0.38 mmol Fe (0.6%) and consumed a maximum of 0.23 mmol (8%) of the acetate. Denitrification, generation of elemental hydrogen, or methane are potentially additional sinks for electrons.

Changes in the material were only noted in the outer layer of the coating with SEM, which suggests that the access to Fe(III) in deeper layers of the coating was restricted by the small micropore sizes and the absence of electron-conducting materials or electron shuttles (Bonneville et al., 2006; Lies et al., 2005). The outer layer is expected to be relevant for fast removal of dissolved  $\text{PO}_4$  from the surrounding solution, and formation at the ICS surface could, hence, limit further adsorption since FeS has a lower sorption capacity than Fe(III)-(hydr)oxides such as ferrihydrite (Kocar et al., 2010). After  $\text{PO}_4$  was reintroduced, 91% was adsorbed in the strongly reducing microcosm while 99% was adsorbed in the other microcosms. Therefore, for the moderately and weakly reducing conditions set in this study, the reductive pressure introduced was not enough to decrease the fast  $\text{PO}_4$  sorption capacity of Fe(III)-(hydr)oxides. However, after longer exposure to strongly reducing conditions, Fe(III)-(hydr)oxide reduction and the formation of secondary minerals such as FeS could eventually become a limiting factor in the performance of ICS filters for  $\text{PO}_4$  retention.

## 5 | CONCLUSION

This research aimed to investigate  $\text{PO}_4$  (im)mobility at the onset of ICS reduction. In the two investigated fields, the ICS filters still removed  $\text{PO}_4$  after 3 yr of use while being subject to metal-reducing conditions. In the microcosm experiment, a range of treatments mimicked the field conditions. For exposure times of 45 d under weakly, moderately, and strongly reducing conditions for ICS with a molar P/Fe ratio of 0.013, P was not released even after Fe and Mn partial reduction. The P sorption capacity of the ICS and its mineral structure remained mostly unchanged after being exposed to moderately and weakly reducing conditions. After moderately

and strongly reducing conditions, we observed the formation of manganese calcium carbonate precipitates in suspension. Only under strongly reducing conditions was a small percentage of Fe transformed into iron sulfides in the outer layer of the Fe coatings. These secondary products could be detrimental to filters by causing filter clogging or by reducing their P sorption capacity. However, our results and the results from earlier work suggest that these detrimental effects only become relevant at operation periods substantially longer than periods of up to 5 yr tested so far.

## ACKNOWLEDGMENTS

This study was funded by P-TRAP (EU Grant No. 813438, Marie Skłodowska-Curie Actions). We would like to thank Delphy and the farmers from the two fields for their participation in this study. We would like to acknowledge Mingkai Ma for XAS sample preparation, Eric Hellebrand for SEM-EDX operation, and Olga Safonova (SLS, PSI) for her help with data acquisition at the SuperXAS beamline, and the SLS is thanked for the allocation of beamtime. Thanks to Menno Tiesma for his help with fieldwork activities.

## AUTHOR CONTRIBUTIONS

Victoria Barcala: Conceptualization; Data curation; Investigation; Methodology; Project administration; Writing – original draft. Stefan Jansen: Conceptualization; Data curation; Formal analysis; Investigation; Methodology; Writing – review & editing. Jan Gerritse: Conceptualization; Formal analysis; Investigation; Methodology; Writing – review & editing. Andreas Voegelin: Conceptualization; Data curation; Formal analysis; Methodology; Writing – review & editing. Stefan Mangold: Data curation; Formal analysis; Resources. Thilo Behrends: Conceptualization; Data curation; Formal analysis; Funding acquisition; Investigation; Methodology; Project administration; Supervision; Writing – review & editing.

## CONFLICT OF INTEREST

The authors declare no conflict of interest.

## ORCID

Victoria Barcala  <https://orcid.org/0000-0002-3245-2867>

Stefan Jansen  <https://orcid.org/0000-0003-4400-0603>

## REFERENCES

- Akhtar, M., Abdelhady, A. L., Azad Malik, M., & O'Brien, P. (2012). Deposition of iron sulfide thin films by AACVD from single source precursors. *Journal of Crystal Growth*, 346(1), 106–112. <https://doi.org/10.1016/j.jcrysgro.2012.02.013>
- Baken, S., Moens, C., Van der Grift, B., & Smolders, E. (2016). Phosphate binding by natural iron-rich colloids in streams. *Water Research*, 98, 326–333. <https://doi.org/10.1016/j.watres.2016.04.032>
- Barcala, V., Rozemeijer, J., Osté, L., Van Der Grift, B., Gerner, L., & Behrends, T. (2020). Processes controlling the flux of legacy phosphorus to surface waters at the farm scale. *Environmental Research Letters*, 16(1), 015003. <https://doi.org/10.1088/1748-9326/abcdd4>
- Bol, R., Gruau, G., Mellander, P. E., Dupas, R., Bechmann, M., Skarbøvik, E., Bieroz, M., Djodjic, F., Glendell, M., Jordan, P., Van der Grift, B., Rode, M., Smolders, E., Verbeeck, M., Gu, S., Klumpp, E., Pohle, I., Fresne, M., & Gascuel-Oudoux, C. (2018). Challenges of reducing phosphorus based water eutrophication in the agricultural landscapes of northwest Europe. *Frontiers in Marine Science*, 5(Aug.), 1–16. <https://doi.org/10.3389/fmars.2018.00276>
- Bonneville, S., Behrends, T., Cappellen, P. V., Hyacinthe, C., & Röling, W. F. M. (2006). Reduction of Fe(III) colloids by *Shewanella putrefaciens*: A kinetic model. *Geochimica et Cosmochimica Acta*, 70(23, Special Issue), 5842–5854. <https://doi.org/10.1016/j.gca.2006.04.029>
- Borch, T., & Fendorf, S. (2008). Phosphate interactions with iron (hydr)oxides: Mineralization pathways and phosphorus retention upon bioreduction. In M. O. Barnett & D. B. Kent (Eds.), *Adsorption of metals by geomedial II: Variables, mechanisms, and model applications* (pp. 321–348). Elsevier. [https://doi.org/10.1016/S1571-9197\(07\)07012-7](https://doi.org/10.1016/S1571-9197(07)07012-7)
- Brewer, P., & Spencer, D. W. (1969). Colorimetric determination of manganese in anoxic waters. *Limnology and Oceanography*, 18(2), 107–110.
- Buijert, A., Talens, R., Chardon, W. J., Groenenberg, J. E., Jansen, S., & Gerritse, J. (2015). *Pilot effectgerichte verwijdering fosfaat bollenstreek*. [https://www.rijnland.net/documents/700/Onderzoeksproject\\_bollensector.pdf](https://www.rijnland.net/documents/700/Onderzoeksproject_bollensector.pdf)
- Chardon, W. J., Groenenberg, J. E., Temminghoff, E. J. M., & Koopmans, G. F. (2012). Use of reactive materials to bind phosphorus. *Journal of Environmental Quality*, 41(3), 636–646. <https://doi.org/10.2134/jeq2011.0055>
- Chardon, W., Groenenberg, J. E., Vink, J. P. M., Voegelin, A., & Koopmans, G. F. (2021). Use of iron-coated sand for removing soluble phosphorus from drainage water. *Science of the Total Environment*, 815, 152738. <https://doi.org/10.1016/j.scitotenv.2021.152738>
- Chardon, W. J., & Schoumans, O. F. (2007). Soil texture effects on the transport of phosphorus from agricultural land in river deltas of northern Belgium, the Netherlands, and north-west Germany. *Soil Use and Management*, 23(Suppl. 1), 16–24. <https://doi.org/10.1111/j.1475-2743.2007.00108.x>
- Csákberényi-Malasics, D., Rodriguez-Blanco, J. D., Kis, V. K., Rečnik, A., Benning, L. G., & Pósfai, M. (2012). Structural properties and transformations of precipitated FeS. *Chemical Geology*, 294–295, 249–258. <https://doi.org/10.1016/j.chemgeo.2011.12.009>
- Griffioen, J. (1994). Uptake of phosphate by iron hydroxides during seepage in relation to development of groundwater composition in coastal areas. *Environmental Science & Technology*, 28(4), 675–681. <https://doi.org/10.1021/es00053a022>
- Groenenberg, J. E., Chardon, W. J., & Koopmans, G. F. (2013). Reducing phosphorus loading of surface water using iron-coated sand. *Journal of Environmental Quality*, 42(1), 250–259. <https://doi.org/10.2134/jeq2012.0344>
- Hansel, C. M., Lentini, C. J., Tang, Y., Johnston, D. T., Wankel, S. D., & Jardine, P. M. (2015). Dominance of sulfur-fueled iron oxide reduction in low-sulfate freshwater sediments. *ISME Journal*, 9(11), 2400–2412. <https://doi.org/10.1038/ismej.2015.50>
- Heiberg, L., Koch, C. B., Kjaergaard, C., Jensen, H. S., & Hansen, H. C. B. (2012). Vivianite precipitation and phosphate sorption following iron reduction in anoxic soils. *Journal of Environmental Quality*, 41(3), 938–949. <https://doi.org/10.2134/jeq2011.0067>



- Hilbrandt, I., Lehmann, V., Zietzschmann, F., Ruhl, A. S., & Jekel, M. (2019). Quantification and isotherm modelling of competitive phosphate and silicate adsorption onto micro-sized granular ferric hydroxide. *RSC Advances*, 9(41), 23642–23651. <https://doi.org/10.1039/c9ra04865k>
- Islam, F. S., Gault, A. G., Boothman, C., Polya, D. A., Chamok, J. M., Chatterjee, D., & Lloyd, J. R. (2004). Role of metal-reducing bacteria in arsenic release from Bengal delta sediments. *Nature*, 430(6995), 68–71. <https://doi.org/10.1038/nature02638>
- Janssen, G. M. C. M., van Walsum, P. E. V., America, I., Pouwels, J. R., Hunink, J. C., Vermeulen, P. T. M., Meshgi, A., Prinsen, G. F., Mulder, N., Visser, M., Kroon, J. T., GMC, P. E. V. v. W., America, I., Pouwels, J. R., Hunink, J. C., Vermeulen, P. T. M., Meshgi, A., Prinsen, G. F., Mulder, N., ... Kroon, T. (2020). *Veranderingsrapportage LHM 4.1: Actualisatie van het lagenmodel, het topsysteem en de bodemplant relaties*. Deltares. [https://nhi.nu/nl/files/5516/1011/9690/11205261-000-BGS-0001\\_-\\_Veranderingsrapportage\\_LHM\\_4.1\\_-\\_definitief\\_2020.pdf](https://nhi.nu/nl/files/5516/1011/9690/11205261-000-BGS-0001_-_Veranderingsrapportage_LHM_4.1_-_definitief_2020.pdf)
- Kocar, B. D., Borch, T., & Fendorf, S. (2010). Arsenic repartitioning during biogenic sulfidization and transformation of ferrihydrite. *Geochimica et Cosmochimica Acta*, 74(3), 980–994. <https://doi.org/10.1016/j.gca.2009.10.023>
- Koopmans, G. F., Hiemstra, T., Vaseur, C., Chardon, W. J., Voegelin, A., & Groenenberg, J. E. (2020). Use of iron oxide nanoparticles for immobilizing phosphorus in-situ: Increase in soil reactive surface area and effect on soluble phosphorus. *Science of the Total Environment*, 711, 135220. <https://doi.org/10.1016/j.scitotenv.2019.135220>
- Kraal, P., van Genuchten, C. M., Behrends, T., & Rose, A. L. (2019). Sorption of phosphate and silicate alters dissolution kinetics of poorly crystalline iron (oxyhydr)oxide. *Chemosphere*, 234, 690–701. <https://doi.org/10.1016/j.chemosphere.2019.06.071>
- Kwon, M. J., O'Loughlin, E. J., Boyanov, M. I., Brulc, J. M., Johnston, E. R., Kemner, K. M., & Antonopoulos, D. A. (2016). Impact of organic carbon electron donors on microbial community development under iron-and sulfate-reducing conditions. *PLOS ONE*, 11(1), e0146689. <https://doi.org/10.1371/journal.pone.0146689>
- Lambert, N., Van Aken, P., Van den Broeck, R., & Dewil, R. (2020). Adsorption of phosphate on iron-coated sand granules as a robust end-of-pipe purification strategy in the horticulture sector. *Chemosphere*, 267, 129276. <https://doi.org/10.1016/j.chemosphere.2020.129276>
- Lies, D. P., Hernandez, M. E., Kappler, A., Mielke, R. E., Gralnick, J. A., & Newman, D. K. (2005). *Shewanella oneidensis* MR-1 uses overlapping pathways for iron reduction at a distance and by direct contact under conditions relevant for biofilms. *Applied and Environmental Microbiology*, 71(8), 4414–4426. <https://doi.org/10.1128/AEM.71.8.4414-4426.2005>
- Loeb, R., Lamers, L. P. M., & Roelofs, J. G. M. (2008). Prediction of phosphorus mobilisation in inundated floodplain soils. *Environmental Pollution*, 156(2), 325–331. <https://doi.org/10.1016/j.envpol.2008.02.006>
- Mellander, P. E., Jordan, P., Shore, M., McDonald, N. T., Wall, D. P., Shortle, G., & Daly, K. (2016). Identifying contrasting influences and surface water signals for specific groundwater phosphorus vulnerability. *Science of the Total Environment*, 541, 292–302. <https://doi.org/10.1016/j.scitotenv.2015.09.082>
- Mendes, L. R. D. (2020). Edge-of-field technologies for phosphorus retention from agricultural drainage discharge. *Applied Sciences (Switzerland)*, 10(2), 634. <https://doi.org/10.3390/app10020634>
- Murphy, J., & Riley, J. P. (1962). A modified single solution method for the determination of phosphate in natural waters. *Analytica Chimica Acta*, 27(C), 31–36. [https://doi.org/10.1016/S0003-2670\(00\)88444-5](https://doi.org/10.1016/S0003-2670(00)88444-5)
- Pedersen, H. D., Postma, D., Jakobsen, R., & Larsen, O. (2005). Fast transformation of iron oxyhydroxides by the catalytic action of aqueous Fe(II). *Geochimica et Cosmochimica Acta*, 69(16), 3967–3977. <https://doi.org/10.1016/j.gca.2005.03.016>
- Penn, C., Chagas, I., Klimeski, A., & Lyngsie, G. (2017). A review of phosphorus removal structures: How to assess and compare their performance. *Water (Switzerland)*, 9(8), 1–22. <https://doi.org/10.3390/w9080583>
- Postma, D., & Appelo, C. A. J. (2000). Reduction of Mn-oxides by ferrous iron in a flow system: Column experiment and reactive transport modeling. *Geochimica et Cosmochimica Acta*, 64(7), 1237–1247.
- Ravel, B., & Newville, M. (2005). ATHENA, ARTEMIS, HEPHAESTUS: Data analysis for X-ray absorption spectroscopy using IFEFFIT. *Journal of Synchrotron Radiation*, 12(4), 537–541. <https://doi.org/10.1107/S0909049505012719>
- Royal Netherlands Meteorological Institute (KNMI). (2022). *Daily weather data in the Netherlands*. <https://www.knmi.nl/nederland-nu/klimatologie/daggegevens>
- Saywell, L. G., & Cunningham, B. B. (1971). Determination of iron colorimetric o-phenanthroline method. *Limnology and Oceanography*, 9, 67–69.
- Schoumans, O. F., Chardon, W. J., Bechmann, M. E., Gascuel-Oudoux, C., Hofman, G., Kronvang, B., Rubæk, G. H., Ulén, B., & Dorioz, J. M. (2014). Mitigation options to reduce phosphorus losses from the agricultural sector and improve surface water quality: A review. *Science of the Total Environment*, 468–469, 1255–1266. <https://doi.org/10.1016/j.scitotenv.2013.08.061>
- Schroth, A. W., Giles, C. D., Isles, P. D. F., Xu, Y., Perzan, Z., & Druschel, G. K. (2015). Dynamic coupling of iron, manganese, and phosphorus behavior in water and sediment of shallow ice-covered eutrophic lakes. *Environmental Science & Technology*, 49, 9758–9767. <https://doi.org/10.1021/acs.est.5b02057>
- Schwertmann, U., & Cornell, R. M. (2000). *Iron oxides in the laboratory: Preparation and characterization*. Wiley. <https://doi.org/10.1176/ajp.2007.164.4.566>
- Senn, A. C., Kaegi, R., Hug, S. J., Hering, J. G., Mangold, S., & Voegelin, A. (2015). Composition and structure of Fe(III)-precipitates formed by Fe(II) oxidation in water at near-neutral pH: Interdependent effects of phosphate, silicate, and Ca. *Geochimica et Cosmochimica Acta*, 162, 220–246. <https://doi.org/10.1016/j.gca.2015.04.032>
- Senn, A. C., Kaegi, R., Hug, S. J., Hering, J. G., Mangold, S., & Voegelin, A. (2017). Effect of aging on the structure and phosphate retention of Fe(III)-precipitates formed by Fe(II) oxidation in water. *Geochimica et Cosmochimica Acta*, 202, 341–360. <https://doi.org/10.1016/j.gca.2016.12.033>
- Sharma, S., Petrushevski, B., & Schippers, J. C. (2002). Characterisation of coated sand from iron removal plant. *Water Science and Technology*, 2(2), 247–257. <https://doi.org/10.2166/ws.2002.0070>
- Sharpley, A., Jarvie, H. P., Buda, A., May, L., Spears, B., & Kleinman, P. (2013). Phosphorus legacy: Overcoming the effects of past management practices to mitigate future water quality impairment. *Journal of Environmental Quality*, 42(5), 1308–1326. <https://doi.org/10.2134/jeq2013.03.0098>
- Skaggs, R. W., Brevé, M. A., & Gilliam, J. W. (1994). Hydrologic and water quality impacts of agricultural drainage. *Critical Reviews in Environmental Science and Technology*, 24(1), 1–32. <https://doi.org/10.1080/10643389409388459>

- Smolders, E., Baetens, E., Verbeeck, M., Nawara, S., Diels, J., Verdriev, M., Peeters, B., De Cooman, W., & Baken, S. (2017). Internal loading and redox cycling of sediment iron explain reactive phosphorus concentrations in lowland rivers. *Environmental Science & Technology*, 51(5), 2584–2592. <https://doi.org/10.1021/acs.est.6b04337>
- Szilas, C. P., Borggaard, O. K., & Hansen, H. C. B. (1998). Potential iron and phosphate mobilization during flooding of soil material. *Water, Air, and Soil Pollution*, 106, 97–109. <https://doi.org/10.1023/A:1004965631574>
- Thamdrup, B. (2000). Bacterial manganese and iron reduction. In *Advances in microbial ecology*. Springer. [https://doi.org/10.1007/978-1-4615-4187-5\\_2](https://doi.org/10.1007/978-1-4615-4187-5_2)
- Van Beek, C. G. E. M., Hofman-Caris, C. H. M., & Zweere, G. J. (2020). Drinking water treatment and chemical well clogging by iron(II) oxidation and hydrous ferric oxide (HFO) precipitation. *Journal of Water Supply: Research and Technology—AQUA*, 69(5), 427–437. <https://doi.org/10.2166/aqua.2020.140>
- Van der Grift, B., Behrends, T., Osté, L. A., Schot, P. P., Wassen, M. J., & Griffioen, J. (2016). Fe hydroxyphosphate precipitation and Fe(II) oxidation kinetics upon aeration of Fe(II) and phosphate-containing synthetic and natural solutions. *Geochimica et Cosmochimica Acta*, 186, 71–90. <https://doi.org/10.1016/j.gca.2016.04.035>
- Vandermoere, S., Ralaizafisoloarivony, N. A., Van Ranst, E., & De Neve, S. (2018). Reducing phosphorus (P) losses from drained agricultural fields with iron coated sand (-glaucanite) filters. *Water Research*, 141, 329–339. <https://doi.org/10.1016/j.watres.2018.05.022>
- Withers, P. J. A., & Haygarth, P. M. (2007). Agriculture, phosphorus, and eutrophication: A European perspective. *Soil Use and Management*, 23, 1–4.
- Young, E. O., & Ross, D. S. (2001). Landscape and watershed processes phosphate release from seasonally flooded soils : A laboratory microcosm study. *Journal of Environmental Quality*, 30, 91–101. <https://doi.org/10.2134/jeq2001.30191x>
- Zhang, Y., Zhu, Z., Liao, Y. G., Dang, Z., & Guo, C. (2021). Effects of Fe(II) source on the formation and reduction rate of biosynthetic mackinawite: Biosynthesis process and removal of Cr(VI). *Chemical Engineering Journal*, 421(P1), 129723. <https://doi.org/10.1016/j.cej.2021.129723>
- Zhu, T., Lai, W., Zhang, Y., & Liu, Y. (2022). Feammox process driven anaerobic ammonium removal of wastewater treatment under supplementing Fe(III) compounds. *Science of the Total Environment*, 804, 149965. <https://doi.org/10.1016/j.scitotenv.2021.149965>
- Zou, X., Wu, Y., Liu, Y., Liu, D., Li, W., Gu, L., Liu, H., Wang, P., Sun, L., & Zhang, Y. (2018). In situ generation of bifunctional, efficient Fe-based catalysts from mackinawite iron sulfide for water splitting. *Chemistry*, 4(5), 1139–1152. <https://doi.org/10.1016/j.chempr.2018.02.023>

## SUPPORTING INFORMATION

Additional supporting information can be found online in the Supporting Information section at the end of this article.

**How to cite this article:** Barcala, V., Jansen, S., Gerritse, J., Mangold, S., Voegelin, A., & Behrends, T. (2023). Phosphorus adsorption on iron-coated sand under reducing conditions. *Journal of Environmental Quality*, 52, 74–87. <https://doi.org/10.1002/jeq2.20432>